

# Catalysis Science & Technology

Accepted Manuscript

This article can be cited before page numbers have been issued, to do this please use: T. J. Eldridge, M. Borchers, P. Lott, J. Grunwaldt and D. E. Doronkin, *Catal. Sci. Technol.*, 2024, DOI: 10.1039/D4CY00574K.



This is an Accepted Manuscript, which has been through the Royal Society of Chemistry peer review process and has been accepted for publication.

Accepted Manuscripts are published online shortly after acceptance, before technical editing, formatting and proof reading. Using this free service, authors can make their results available to the community, in citable form, before we publish the edited article. We will replace this Accepted Manuscript with the edited and formatted Advance Article as soon as it is available.

You can find more information about Accepted Manuscripts in the [Information for Authors](#).

Please note that technical editing may introduce minor changes to the text and/or graphics, which may alter content. The journal's standard [Terms & Conditions](#) and the [Ethical guidelines](#) still apply. In no event shall the Royal Society of Chemistry be held responsible for any errors or omissions in this Accepted Manuscript or any consequences arising from the use of any information it contains.

Processed data supporting conclusions is available in the manuscript and the Supporting Information. Raw data can be provided by the authors upon a reasonable request.

View Article Online

DOI: 10.1039/D4CY00574K

Open Access Article. Published on 25 June 2024. Downloaded on 6/26/2024 10:06:59 AM.  
This article is licensed under a Creative Commons Attribution 3.0 Unported Licence.



## ARTICLE

## Elucidating the Role of the State of Pd in the H<sub>2</sub>-SCR of NO<sub>x</sub> by Operando XANES and DRIFTS

Thomas J. Eldridge<sup>a,b,\*</sup>, Michael Borchers<sup>b</sup>, Patrick Lott<sup>b</sup>, Jan-Dierk Grunwaldt<sup>a,b</sup>, Dmitry E. Doronkin<sup>a,b,\*</sup>

Received 00th January 20xx,  
Accepted 00th January 20xx

DOI: 10.1039/x0xx00000x

The selective catalytic reduction (SCR) of NO<sub>x</sub> with hydrogen is an attractive strategy for NO<sub>x</sub> removal when H<sub>2</sub> is used as a sustainable fuel in combustion engines. However, the pathway suffers from a strong overconsumption of H<sub>2</sub> via direct oxidation to water. In order to improve the understanding of the SCR mechanism with H<sub>2</sub> as the reductant, the state of the active metal, the reactive surface intermediates, and the conditions which are suited for efficient SCR need to be uncovered. A 1%Pd/5%V<sub>2</sub>O<sub>5</sub>/20%TiO<sub>2</sub>-Al<sub>2</sub>O<sub>3</sub> catalyst was investigated using *operando* X-ray absorption spectroscopy (XAS) and diffuse reflectance infrared Fourier-transform spectroscopy (DRIFTS) to track the temperature dependent structure and state of Pd, as well as its gradients and surface intermediates. XAS shows that NO reduces oxidized Pd, forming metal-support interfacial nitrates according to DRIFTS. Partially reduced Pd becomes oxidized by reducing interfacial NO<sub>x</sub> species to Pd-nitrosyls. Limitations for the H<sub>2</sub>-SCR of NO<sub>x</sub> arise from the balance of adsorbed Pd-NO and activated H<sub>2</sub>, which is dependent on Pd state. The bulk metallic Pd which forms above 250 °C causes a runaway activation of H<sub>2</sub>, further reduction of Pd, and loss of nitrosyls on Pd. The highest activity occurs when Pd is oxidized enough to promote metal-support interfacial nitrates and also reduced enough to convert these nitrates to Pd-nitrosyls. The storage of NO<sub>x</sub> and formation of NH<sub>x</sub> on vanadia-titania permits conversion of NO at high temperatures, but does not counteract the deactivation of Pd. In conclusion, activation of H<sub>2</sub> is favored on metallic sites, but must be moderated to allow for PdO being present as well.

### Introduction

In the course for reducing carbon-based engine-out emissions and because of its potential future production from sustainable sources,<sup>1, 2</sup> hydrogen has been investigated as an attractive alternative to diesel in thermal combustion engines. Apart from being a potential sustainable energy carrier, the primary motivation for using H<sub>2</sub> is the avoidance of carbon and particulate matter (PM) emissions in the exhaust. However, under the high temperatures of H<sub>2</sub> combustion, N<sub>2</sub> oxidation by O<sub>2</sub> from air leads to NO<sub>x</sub> as a pollutant in the 1000 ppm range. While these NO<sub>x</sub> emissions can be mitigated by optimal air-to-fuel ratios and engine control methods,<sup>3-5</sup> H<sub>2</sub> thermal combustion engines have a higher NO<sub>x</sub> emission potential relative to traditional fuels.<sup>6</sup>

In order to meet NO<sub>x</sub> emission guidelines, an emission-out catalyst for the selective catalytic reduction (SCR) of NO<sub>x</sub> is necessary. At present, SCR of NO<sub>x</sub> is largely executed using NH<sub>3</sub> as the reductant.<sup>7-13</sup> However, due to the direct availability from the fuel tank, H<sub>2</sub> has been investigated as an alternative SCR agent.

Current catalysts for SCR of NO<sub>x</sub> by H<sub>2</sub> show higher levels of NO<sub>x</sub> conversion, relative to NH<sub>3</sub> as the reducing agent, at lower temperatures.<sup>14, 15</sup> However, the primary challenge of H<sub>2</sub>-SCR is combatting the competitive direct oxidation of H<sub>2</sub> to H<sub>2</sub>O, which becomes the favored reaction pathway at high temperatures. Further complications include several reactions simultaneously occurring over the catalyst bed, including NH<sub>3</sub> formation and subsequent NH<sub>3</sub>-SCR, leading to gradients in reaction product concentrations and in catalyst structure.<sup>16, 17</sup>

Supported noble metal catalysts, with favor towards Pt<sup>18-23</sup> and Pd<sup>24-29</sup>, are most widely investigated for H<sub>2</sub>-SCR. Pt and Pd present different benefits and challenges relative to other noble metals: where Pt shows substantially higher NO<sub>x</sub> conversion but lower selectivity for N<sub>2</sub> with respect to N<sub>2</sub>O, and where Pd has high selectivity for N<sub>2</sub> but lower overall catalytic activity.<sup>15</sup>

There are several primary groups of catalyst supports that have been studied in H<sub>2</sub>-SCR: (1) TiO<sub>2</sub>,<sup>28-32</sup> often combined with V<sub>2</sub>O<sub>5</sub>,<sup>26, 27, 33, 34</sup> (2) WO<sub>3</sub>/ZrO<sub>2</sub>,<sup>35-38</sup> and (3) MgO-CeO<sub>2</sub>,<sup>19-21</sup> and (4) zeolites, alone or in combination with other supports.<sup>39-43</sup> H<sub>2</sub>-SCR catalysts with low noble metal loadings (< 1 wt. %) of Pt or Pd on WO<sub>3</sub>/ZrO<sub>2</sub> or MgO-CeO<sub>2</sub> have shown wide temperature ranges (100 to 400 °C) of NO<sub>x</sub> conversion with high (> 80%) selectivity for N<sub>2</sub>. However, they have not been studied as extensively as catalysts supported on TiO<sub>2</sub>. Pd on TiO<sub>2</sub>-Al<sub>2</sub>O<sub>3</sub> is notable for converting NO<sub>x</sub> over a wide temperatures range from 100 to 350 °C, but with a significant drop in activity at 200 °C.<sup>26, 30</sup> This phenomenon was explained by NO reduction to N<sub>2</sub>, occurring from 100 to 200 °C, NO oxidation to NO<sub>2</sub>, occurring

<sup>a</sup> Institute of Catalysis Research and Technology, Karlsruhe Institute of Technology, Eggenstein-Leopoldshafen 76344, Germany

<sup>b</sup> Institute for Chemical Technology and Polymer Chemistry, Karlsruhe Institute of Technology, Karlsruhe 76131, Germany

\* corresponding author

Electronic Supplementary Information (ESI) available: [details of any supplementary information available should be included here]. See DOI: 10.1039/x0xx00000x



from 200 to 400 °C, and NO<sub>2</sub> reduction to N<sub>2</sub> at 100 to 400 °C. The addition of V<sub>2</sub>O<sub>5</sub> to Pd/TiO<sub>2</sub>-Al<sub>2</sub>O<sub>3</sub> followed a study with Pd/V<sub>2</sub>O<sub>5</sub>/Al<sub>2</sub>O<sub>3</sub> which showed high levels of NO reduction to N<sub>2</sub> in the narrow range of 200 to 300 °C,<sup>33</sup> which well counteracted the observed activity decrease on Pd/TiO<sub>2</sub>-Al<sub>2</sub>O<sub>3</sub>.<sup>26</sup>

In order to better understand the reactive conditions of Pd/V<sub>2</sub>O<sub>5</sub>/TiO<sub>2</sub>-Al<sub>2</sub>O<sub>3</sub> for H<sub>2</sub>-SCR of NO<sub>x</sub>, a study was performed using a honeycomb monolith and a variety of concentrations of NO, H<sub>2</sub>, and O<sub>2</sub>.<sup>34</sup> It was shown that the H<sub>2</sub> reaction pathway plays a significant role, where NO reduction to N<sub>2</sub> occurred more readily when either H<sub>2</sub> amounts were increased or O<sub>2</sub> concentration decreased, as O<sub>2</sub> competes with NO for reaction with H<sub>2</sub>. Additionally, the catalyst state (e.g. Pd oxidized/reduced, Pd particles or clusters) was shown to play a significant role in SCR activity, as the pre-reduced catalyst showed significantly higher activity and N<sub>2</sub> selectivity at temperatures below 200 °C.

In order to gain further insight into the surface reactions and the mechanism, ex-situ characterization and catalytic activity studies, which use outlet gas beyond the catalyst, are not sufficient for observing what occurs within the black-box catalyst. For this purpose, *operando* and *in-situ* characterization is needed to unravel the species and structure of the catalyst as a function of time and space while the reaction is ongoing.<sup>44</sup> Spectroscopic techniques, such as X-ray absorption spectroscopy (XAS) and diffuse reflectance infrared Fourier-transformed spectroscopy (DRIFTS) are able to measure the bulk and surface state of catalysts during steady-state and transient chemical reactions. These techniques also enable the measurement of spatial gradients in surface species concentration and catalyst state<sup>45-47</sup> and are thus applied during H<sub>2</sub>-SCR in this study. Herewith, the present work aims at linking the oxidation state of Pd to the catalytic hydrogen combustion and selective catalytic reduction of NO<sub>x</sub> by H<sub>2</sub> under dynamic reaction conditions. Both *operando* spatially and time-resolved XAS and *operando* DRIFTS measurements were conducted on a 1%Pd/V<sub>2</sub>O<sub>5</sub>/TiO<sub>2</sub>-Al<sub>2</sub>O<sub>3</sub> catalyst.

## Experimental

A 1%Pd/5%V<sub>2</sub>O<sub>5</sub>/20%TiO<sub>2</sub>-Al<sub>2</sub>O<sub>3</sub> catalyst was prepared via the following steps: γ-Al<sub>2</sub>O<sub>3</sub> (Puralox, Sasol) was calcined in air for 5 h at 700 °C and suspended in a solution of Ti(OBu)<sub>4</sub> (Merck) and EtOH (≥99.8%, VWR Chemicals); Ti(OBu)<sub>4</sub> was hydrolyzed by dropwise addition of deionized water to the suspension and rigorous stirring. The received TiO<sub>2</sub>-Al<sub>2</sub>O<sub>3</sub> solid was dried for 2 h at 70 °C and calcined in air for 6 h at 500 °C. V<sub>2</sub>O<sub>5</sub> was added to the 20 wt. % TiO<sub>2</sub>-Al<sub>2</sub>O<sub>3</sub> support via incipient wetness impregnation (IWI) using a NH<sub>4</sub>VO<sub>3</sub> (Alfa Aesar) solution with aqueous oxalic acid (Merck) and subsequent drying for 1 h at 70 °C and calcination in air for 12 h at 500 °C. Pd was added in a second IWI using an aqueous Pd(NH<sub>3</sub>)<sub>4</sub>(NO<sub>3</sub>)<sub>2</sub>-solution (abcr) and calcination of the received catalyst powder for 16 h at 500 °C. Inductively coupled plasma optical emission spectroscopy (ICP-OES) confirmed the target elemental composition of the catalyst.

N<sub>2</sub>-physisorption of the catalyst powder was measured using a BELSORP-mini II instrument (BEL Japan) with pretreatment under vacuum at 300 °C for 2 h. Analysis of the adsorption-desorption curve by the Brunauer-Emmett-Teller (BET) method yielded the specific surface area and total pore volume of the catalyst.

X-ray diffraction (XRD) patterns were acquired with an X'PERT PRO diffractometer (PANalytical) using a Cu-Kα radiation source with a wavelength of 1.54 Å (2θ from 20 to 80°, step size of 0.017°, acquisition time of 0.44 s per data point).

Temperature-programmed reduction by hydrogen (H<sub>2</sub>-TPR) was performed from 40 to 600 °C at 10 K min<sup>-1</sup> in a 50 mL min<sup>-1</sup> flow of 10% H<sub>2</sub> in Ar using an AutoChem II Chemisorption Analyzer (Micromeritics). A thermal conductivity detector (TCD) measured H<sub>2</sub> consumption. Prior to H<sub>2</sub>-TPR, the sample was pretreated by heating with a temperature ramp of 10 K min<sup>-1</sup> up to 500 °C under 20% O<sub>2</sub> in N<sub>2</sub>.

*Operando* X-ray absorption spectroscopy (XAS) measurements were obtained at the PETRA III P64 beamline<sup>48</sup> at DESY (Hamburg, Germany). Catalyst powder was pressed and sieved to 125-250 μm grains to minimize mass transport limitations. The sieved fraction was placed between two quartz wool plugs in a fixed-bed quartz capillary serving as plug-flow microreactor.<sup>49</sup> The microreactor was heated by a hot air gas blower (Leister LE mini kit). Using capillary microreactors of 2 mm outer diameter and 0.02 mm wall thickness loaded with 12.5 mg of the granulated catalyst for a bed length of 4.1 mm, NO conversion was measured by a mass spectrometer (MS, Hiden ExQ) at the outlet, while simultaneously recording time-resolved X-ray absorption near edge structure (XANES) spectra at different positions along the catalyst bed, under a 50 mL/min flow (GHSV 60,000 h<sup>-1</sup>) of 1000 ppm NO, 5000 ppm H<sub>2</sub>, and 10% O<sub>2</sub> (He balance) in different gas combinations, following the sequential order as shown in Table 1; between each gas mixture, the setup pipes and the reactor itself were flushed with He. The sample was oxidized in 10% O<sub>2</sub> at 500 °C prior to TPR. A single light-off-light-out cycle from 25 to 350 °C at 2 K/min was performed for each gas mixture during continuous XANES measurements.

**Table 1.** Volumetric inlet gas compositions for the XANES/DRIFTS catalytic activity measurements (He/Ar balance), provided in the order (top-to-bottom) introduced to the Pd/V<sub>2</sub>O<sub>5</sub>/TiO<sub>2</sub>-Al<sub>2</sub>O<sub>3</sub> catalyst.

Gas Mix	NO (ppm)	H <sub>2</sub> (ppm)	O <sub>2</sub> (%)
TPO	0	0	10
NOA	1000	0	10
SCR	1000	5000	10
MixA	0	5000	10
NOB	1000	0	0
MixB	1000	5000	0
TPR	0	5000	0



Due to time limitations at the XAS beamline, only two-point calibrations (zero gas and educts at zero conversion) of MS instrumentation were possible and allowed for only qualitative and semi-quantitative analysis. Additionally, small quantities (i.e. < 100 ppm) of nitrogen species such as  $\text{NH}_3$ ,  $\text{N}_2$ ,  $\text{N}_2\text{O}$ , and  $\text{NO}_2$  measured at  $m/z$  values of 15, 28, 44, and 46 were particularly difficult to detect by MS and did not produce enough counts for robust quantitative analysis.

Quick extended X-ray absorption fine structure (QEXAFS) spectra<sup>50</sup> were obtained with a monochromator frequency of 1 Hz, resulting in 2 spectra per second. The polychromatic X-ray beam from the tapered undulator was tuned to the Pd K edge by a liquid nitrogen cooled Si(111) channel-cut crystal monochromator. With a beam size of 1.0 mm (horizontal) x 1.0 mm (vertical), 4 points along the catalyst bed were measured. For the spatially resolved XANES evaluation, the positions were continuously cycled during light-off and the constantly running QEXAFS measurements, holding at each position for 30 seconds; timestamps were recorded before and after each movement of the reactor to isolate and average spectra obtained at each position in order to improve the signal quality. Pd foil measured simultaneously with the catalyst served as the reference.

For evaluation of the XANES spectra, the QEXAFS data were read-in, split, and exported as text files using the JAQ Analyzes QEXAFS software (version 5.3).<sup>48</sup> Using a Python (version 3.10) script empowered by the Larch (version 0.9.65) package,<sup>51</sup> XANES spectra were calibrated for energy, sorted and averaged by position, and correlated with light-off temperature values. Normalization of spectra and subsequent linear combination analysis (LCA) were performed using the Athena software from the Demeter software package (version 0.9.26),<sup>52</sup> across an energy range from 24340 to 24400 eV, using the as-prepared Pd/V<sub>2</sub>O<sub>5</sub>/TiO<sub>2</sub>-Al<sub>2</sub>O<sub>3</sub> catalyst in oxygen and H<sub>2</sub> after temperature-programmed oxidation and reduction at 350 °C, respectively, as references.

DRIFTS spectra were obtained using a Vertex 70 spectrometer (Bruker) equipped with a Praying Mantis mirror assembly (Harrick) and a liquid nitrogen cooled mercury cadmium telluride (MCT) detector with a resolution of 4 cm<sup>-1</sup>. A Praying Mantis high temperature reaction chamber (Harrick) with flat CaF<sub>2</sub> windows was loaded with 24.5 mg granulated catalyst (125 - 250 μm). Steady-state DRIFTS spectra were recorded as an average of 300 scans at 40 kHz at 25 °C intervals from 50 to 325 °C, approximating a single light-off-light-out cycle, with a flow of 50 ml/min (GHSV 30,000 h<sup>-1</sup>) using the same pretreatment, gas mixtures, and sequence as with the XAS measurements and as described in Table 1, but using argon instead of helium for balance. Background reference interferograms were collected at each temperature once during cooling down after the initial oxidation pretreatment (10% O<sub>2</sub>, 325 °C, 30 min). For DRIFTS quantitative analysis and comparison, the baseline of the pseudo-absorbance spectra was zeroed and flattened using a piecewise cubic Hermite interpolating polynomial (PCHIP) function.

## Results and discussion

View Article Online

DOI: 10.1039/D4CY00574K

### Characterization and Catalytic Activity of Pd/V<sub>2</sub>O<sub>5</sub>/TiO<sub>2</sub>-Al<sub>2</sub>O<sub>3</sub>

The characterization data, light-off conversion profiles, product selectivity, and reaction pathway selectivity for this catalyst have previously been reported in great detail on the same catalyst coated on a honeycomb.<sup>34</sup> Hence, the results reported herein are discussed with respect to the outlet mass spectrometer measurements for the purpose of relating data from the XAS and DRIFTS measurements to the activity profile in the specific *operando* measurements. Figures 1a and 1b show the light-off curves for NO reduction in the presence of H<sub>2</sub> and the H<sub>2</sub>-SCR of NO, respectively.

The atypical light-off observed in Figure 1a is due to the absence of O<sub>2</sub>, matching well with the honeycomb study which showed that the NO conversion curve broadens and shifts to lower temperatures when the ratio of O<sub>2</sub> to H<sub>2</sub> is lowered. Overstoichiometric conversion of H<sub>2</sub> and the gradual increase in H<sub>2</sub>O MS intensity in the absence of NO during NO reduction by H<sub>2</sub>, as shown in Figure 1a, is due to the broad reduction area from 200 to 600 °C previously shown<sup>34</sup> by H<sub>2</sub>-TPR for this catalyst. The change in the MS zero line for N<sub>2</sub>O suggests conversion of trace N<sub>2</sub>O impurities present in the NO gas cylinder available at the synchrotron.

Due to inherent differences between testing monolith and powder catalysts, under identical SCR gas conditions, the powder catalyst of this study underwent light-off for NO and H<sub>2</sub> conversion at higher temperatures relative to the monolith catalyst (cf. Figure 1b); however, it is possible to correlate changes in the Pd state and surface species with the light-off and relate these data to the previously reported honeycomb catalyst study. This will be discussed in more detail below in combination with DRIFTS and XAS analysis below.

With exception to N<sub>2</sub>O in Figure 1a, nitrogen species products formed in amounts below the detection limit of the MS instrumentation; however, product selectivity under these gas conditions has been previously reported<sup>34</sup> and is out of the scope of this study. MS data measured during other gas conditions are shown in Figure S1. The relatively low O<sub>2</sub> conversion in Figure 1b is due to the stoichiometric excess of O<sub>2</sub> used; Figure S2 shows the absolute concentrations of H<sub>2</sub>, NO, and O<sub>2</sub>. From these data, a slight delay between the onset of SCR activity at 200 °C and increased O<sub>2</sub> conversion at 230 °C was observed, at which point the conversion of NO stagnated. This matches well with previous findings with the honeycomb catalyst where it was concluded that the direct oxidation of H<sub>2</sub> predominantly opposes H<sub>2</sub>-SCR activity at elevated temperatures.

### *Operando* XANES Measurements

In order to elucidate the dynamic changes in the Pd oxidation state during H<sub>2</sub>-SCR over the 1%Pd/5%V<sub>2</sub>O<sub>5</sub>/20%TiO<sub>2</sub>-Al<sub>2</sub>O<sub>3</sub> catalyst, QEXAFS measurements were performed with different gas mixtures. The resulting XANES spectra were quantified by LCA using corresponding reference spectra. Reference spectra for metallic/reduced Pd and oxidized Pd were obtained from 5000 ppm H<sub>2</sub> in argon (TPR) and 10% O<sub>2</sub> in argon



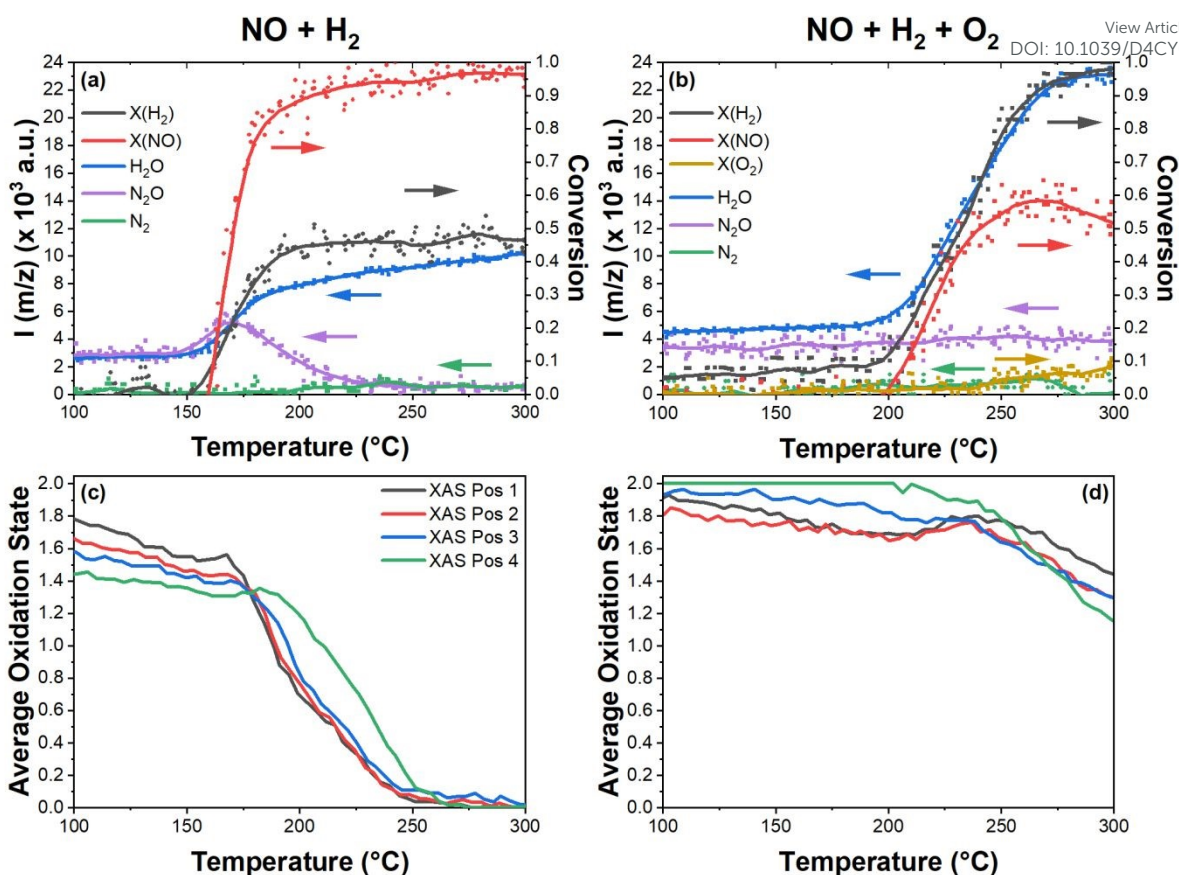


**Fig. 1** Light off curves on 1%Pd/5%V<sub>2</sub>O<sub>5</sub>/20%TiO<sub>2</sub>-Al<sub>2</sub>O<sub>3</sub> (heating ramp of 2 K/min, 50 mL/min / GHSV 60,000 h<sup>-1</sup>) during conversion of H<sub>2</sub>, NO, and O<sub>2</sub> to H<sub>2</sub>O, N<sub>2</sub>, and N<sub>2</sub>O (MS intensities at m/z = 2, 30, and 32 and 18, 28, and 44, respectively) in (a) 1000 ppm NO, 5000 ppm H<sub>2</sub> in He and (b) 1000 ppm NO, 5000 ppm H<sub>2</sub>, and 10% O<sub>2</sub> in He (SCR); the dots are experimental data and the solid lines are locally weighted scatterplot smoothing (LOWESS) regressions; (c, d)

(TPO) measurements, as shown in the ESI by Figure S3; LCA fits for these spectra were done using Pd foil and PdO references to confirm the catalyst had fully reduced and oxidized during TPR and TPO, respectively. Further analysis of the extended X-ray absorption fine structure (EXAFS) of the fully reduced Pd yielded

an average Pd coordination number of 8.1 (cf. Table S1), corresponding to nanoparticles of approximately 1 nm in diameter assuming a fcc full truncated cubooctahedral particle.<sup>53</sup>

Sample XANES spectra for the H<sub>2</sub>-SCR (1000 ppm NO, 5000

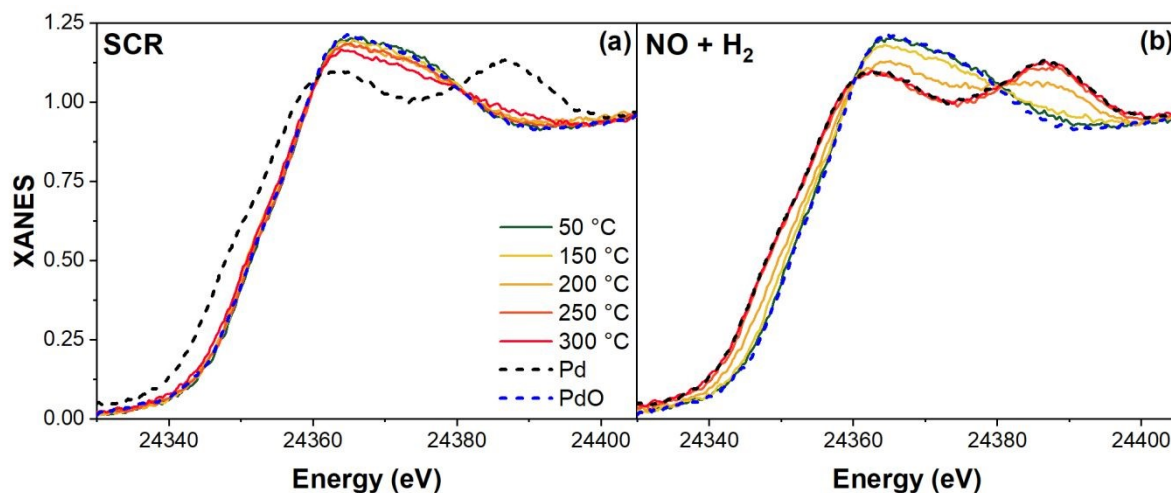


**Fig. 2** Temperature dependent XANES spectra at the Pd K-edge for the 1%Pd/5%V<sub>2</sub>O<sub>5</sub>/20%TiO<sub>2</sub>-Al<sub>2</sub>O<sub>3</sub> catalyst during the (a) 1000 ppm NO, 5000 ppm H<sub>2</sub>, and 10% O<sub>2</sub> in Ar (H<sub>2</sub>-SCR) and (b) 1000 ppm NO and 5000 ppm H<sub>2</sub> in Ar.



ppm H<sub>2</sub>, and 10% O<sub>2</sub> in argon) and NO reduction (1000 ppm NO and 5000 ppm H<sub>2</sub> in argon) gas conditions along with metallic Pd and PdO reference spectra are shown in Figure 2. The LCA fits to these spectra are shown in Figures 1c and 1d for the SCR and NO reduction conditions, respectively, showing space-resolved dynamic changes in the average oxidation state of Pd.

In the SCR reaction mixture, Pd is mostly in the oxidized state (Figure 1d), gradually reducing with increasing temperature from 50 to 200 °C, with the beginning of the catalyst bed more reduced than the end. At the onset of SCR activity at 200 °C, the catalyst front oxidizes slightly, matching the conversion curve of NO shown in Figure 1b. A local maxima of oxidation was reached at 250 °C, correlating with the maximum NO conversion. The subsequent Pd reduction matches the decrease in NO conversion from 250 to 300 °C. Spatially, the front of the catalyst bed reduces more from 50 to 200 °C and the end is generally more oxidized before the onset of SCR activity at 200 °C. From 200 to 300 °C, an inversion occurs such that the end of the catalyst bed is more reduced than the front. In the absence of DRIFTS data, the increase in Pd oxidation state during NO conversion suggests that Pd assists H<sub>2</sub> in the reduction of adsorbed NO species leading to the formation of N<sub>2</sub>O or N<sub>2</sub>. When considering the competing oxidation and reduction of Pd by O<sub>2</sub> and H<sub>2</sub>, respectively, the alternate explanation for the oxidation of Pd from 200 to 250 °C is the loss of H<sub>2</sub> due to conversion during the H<sub>2</sub>-SCR reaction. However, this is not likely to be the case. The substantial reduction of Pd above 250 °C, which was not observed with the NO + O<sub>2</sub> and H<sub>2</sub> + O<sub>2</sub> gas conditions (cf. Figure S3), indicates that H<sub>2</sub> and NH<sub>x</sub> continue to reduce Pd even when participating in separate reactions. While the oxidation of Pd by O<sub>2</sub> is sufficient to counteract PdO reduction by H<sub>2</sub>, reduced NH<sub>x</sub> species limit the reoxidation of Pd by O<sub>2</sub>. The role of NO in the oxidation of Pd will be discussed in further detail in the DRIFTS analysis below.

For the NO reduction condition (without O<sub>2</sub>), at lower temperatures (50 to 150 °C) Pd is slightly reduced yet mostly oxidized with an average oxidation state of ~1.6 (Figure 1c), with the end of the catalyst more reduced than the front. Pd gradually reduces in the presence of NO and H<sub>2</sub> until 168 °C where all positions rapidly reduce to Pd<sup>0</sup>, with a temperature-dependent delay ( $\Delta T$ ) of 5 and 32 °C towards the end of the catalyst bed at positions 3 and 4, respectively. The onset of NO conversion occurs at 150 °C (before the rapid reduction in Pd, cf. MS data shown in Figure 1a). Instead of correlating directly with NO reduction, the Pd oxidation state profile matches the diminishing production of N<sub>2</sub>O. This suggests that H<sub>2</sub> partially reduces NO to N<sub>2</sub>O in the process of reducing Pd, either directly or via an intermediate. The space-resolved average oxidation states of Pd according to LCA fits for gas conditions of 1000 ppm NO in argon and 1000 ppm NO and 10% O<sub>2</sub> in argon can be found in the supplementary information (Figure S3).

As XAS is a bulk sensitive technique, detailed mechanisms cannot be drawn solely from these data. In order to complement these measurements and provide a more complete insight into the mechanism under these dynamic

conditions, the role of surface intermediates has been investigated in more detail by DRIFTS. DOI: 10.1039/D4CY00574K

### Operando DRIFTS Measurements

**Adsorption of NO.** In order to identify the adsorbed NO species in the absence of any other reactive gases, DRIFTS measurements under a flow of NO and argon were performed (the uncorrected spectra are given in Figure S4). Several bands were found (summary given in Figure 3), with high frequency species at 3777, 3733, 3691, and 3658 cm<sup>-1</sup>, a broad water peak between 2500 and 3500 cm<sup>-1</sup>, middle frequency bands at 2181, 2111, 2047, 1868, 1820, 1813, 1776, and 1745 cm<sup>-1</sup>, and lower frequency bands at 1680, 1647, 1620, 1581, 1545, 1488, 1310, and 1270 cm<sup>-1</sup>.

The negative bands between 3500 and 3800 cm<sup>-1</sup> are assigned to OH-species,  $\nu(\text{OH})$ ,<sup>54-56</sup> with the 3733 and 3691 cm<sup>-1</sup> bands associated with a loss of Ti<sup>4+</sup>-OH and the 3658 cm<sup>-1</sup> band with a loss of V-OH species. The bands associated with Ti-OH are more intense than those for V-OH. These bands become less intense at higher temperature, following the gradual disappearance of the broad water peak. The negative band at 2047 cm<sup>-1</sup> is associated with  $2\nu(\text{V}=\text{O})$  overtones and a loss of V<sup>5+</sup> species within the catalyst.<sup>56, 57</sup>

Bands at 2181 and 2111 cm<sup>-1</sup> have generally been assigned to NO<sup>+</sup> on TiO<sub>2</sub> catalysts and linked to NO adsorption on Brønsted acid sites as a replacement of H<sup>+</sup> in OH species.<sup>58, 59</sup> These bands are very weak relative to other bands (Figure 4a) but are present in the greatest amount at temperatures where nitrates are more prevalent than Pd-adsorbed nitrosyls (Pd-NO), as described below. They are indicative of an oxidizing environment for NO. The band at 2181 cm<sup>-1</sup> increases in intensity up to 175 °C before decreasing and disappearing by 250 °C, whereas the 2111 cm<sup>-1</sup> band is most pronounced at 50 °C and vanishes above 175 °C. Both peaks redshift with increasing temperature, suggesting slight relaxation of the N-O bonds due to reduced constraints localized around the surface binding site.

The bands between 1725 and 1900 cm<sup>-1</sup> are associated with linearly adsorbed NO on Pd and V, which have been previously reported at 1890 (V<sup>4+</sup> (NO)<sub>2</sub>,  $\nu_s(\text{NO})$ )<sup>60</sup> and Pd<sup>2+</sup> (NO)<sub>2</sub>,  $\nu_s(\text{NO})$ )<sup>61</sup>, 1828 (V<sup>3+</sup> (NO)<sub>2</sub>,  $\nu_s(\text{NO})$ )<sup>56</sup> 1830 (Pd<sup>2+</sup>,  $\nu(\text{N}=\text{O})$ )<sup>59</sup> 1776 (V<sup>4+</sup> (NO)<sub>2</sub>,  $\nu_{as}(\text{NO})$ )<sup>62</sup> and Pd<sup>+</sup>,  $\nu(\text{NO})$ )<sup>55</sup>, and 1745 cm<sup>-1</sup> (V<sup>4+</sup> (NO)<sub>2</sub>,  $\nu_{as}(\text{NO})$ )<sup>56</sup> and Pd<sup>0</sup>,  $\nu(\text{NO})$ )<sup>55</sup>. While there is potential overlap between Pd-NO and V-NO species, IR bands of nitrosyls are only seen on vanadium at or above ambient temperatures after substantial reduction of the catalyst.<sup>56</sup> A previous DRIFTS study by Macleod *et al.* on V<sub>2</sub>O<sub>5</sub>/Al<sub>2</sub>O<sub>3</sub> with and without Pd concluded that V<sup>3+</sup> and V<sup>4+</sup> centers do not form under H<sub>2</sub>-SCR conditions (4000 ppm H<sub>2</sub>, 500 ppm NO, 5% O<sub>2</sub>), while also measuring a negative V<sup>5+</sup> band at 2047 cm<sup>-1</sup>.<sup>33</sup> Likewise, only nitrosyl bands for the Pd loaded catalyst were observed, and hence the bands at 1819 and 1788 cm<sup>-1</sup> were assigned to Pd<sup>+</sup>-NO. Considering these findings, it is reasonable to conclude that the bands between 1725 and 1900 cm<sup>-1</sup> in the current study are predominantly due to NO species adsorbed on Pd.



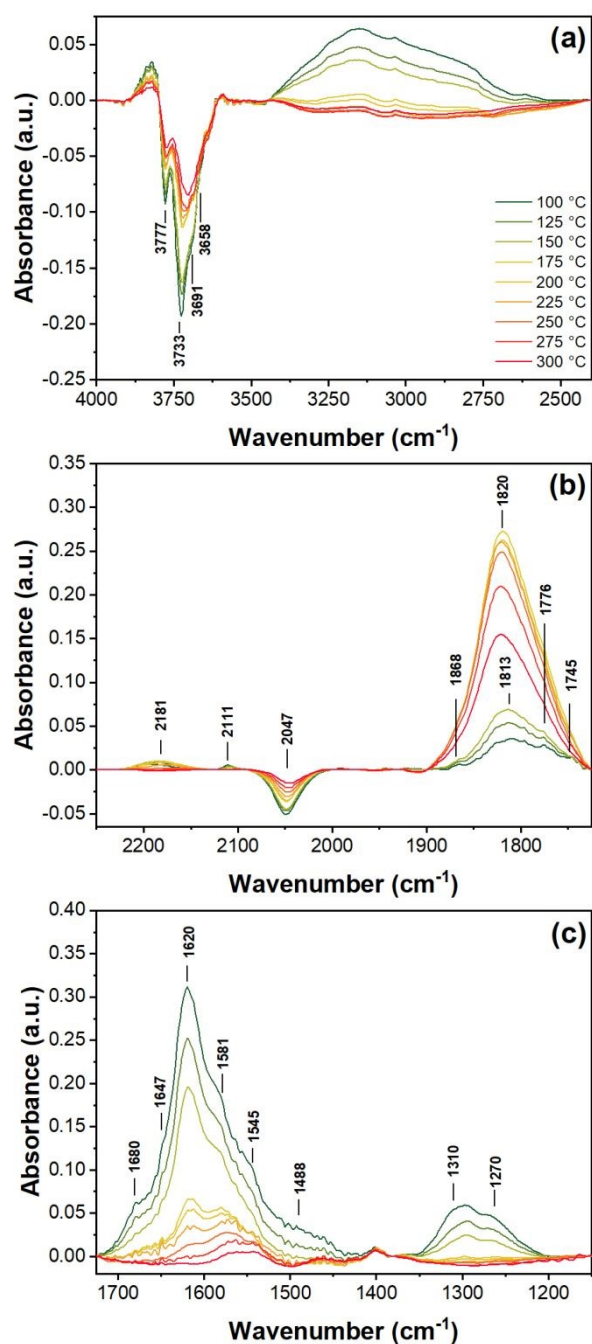


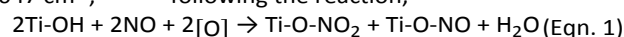
**Fig. 3** Temperature dependent DRIFTS spectra of the 1%Pd/5%V<sub>2</sub>O<sub>5</sub>/20%TiO<sub>2</sub>-Al<sub>2</sub>O<sub>3</sub> catalyst under a flow of 1000 ppm NO in Ar, shown at (a) high wavenumbers for OH (negative) and water bands, (b) middle wavenumbers for NO<sup>+</sup>, V=O (negative), and Pd-NO bands, and (c) low wavenumbers for support nitrate and nitrite bands.

In the case of the measurements reported herein, at low temperatures for the adsorption of NO on Pd, the peak at 1813 cm<sup>-1</sup> (Pd<sup>n+</sup>, Pd<sup>2+</sup>(OH)NO,  $\nu(\text{NO})$ )<sup>63</sup> is the predominant band. The blueshift of this peak to 1820 cm<sup>-1</sup>, which occurred with increasing temperature, may be due to overlap among a combination of lesser bands at 1830 and 1828 cm<sup>-1</sup> with the 1813 cm<sup>-1</sup> band, suggesting a greater prevalence of Pd<sup>2+</sup>. This

corresponds to the slight oxidizing effect of NO on Pd when Pd is sufficiently reduced as seen by XAS (cf. Figure S2e). However, the dominance and symmetry of the 1820 cm<sup>-1</sup> band above 150 °C makes it difficult to assign direct contribution of additional nitrosyl states under these conditions. At lower temperatures from 100 to 150 °C, weaker bands at 1745, 1776, and 1868 cm<sup>-1</sup> may contribute asymmetry to the 1813 cm<sup>-1</sup> band, as they are significant features observed under other gas conditions discussed in later sections below, but are not significant features during NO adsorption on this catalyst. At approximately 250 °C, the band intensity of Pd-NO moieties begins to decrease sharply. At these high temperatures, according to previous temperature programmed desorption (TPD) measurements of NO on Pd,<sup>64</sup> the rate of desorption of NO from Pd limits the presence of adsorbed nitrosyl species.

The negative band area at 2047 cm<sup>-1</sup> decreases in unison with the shrinking of negative OH bands (3500-3800 cm<sup>-1</sup>) and of low frequency bands from 1200 to 1650 cm<sup>-1</sup>, which are assigned to different nitrate species ( $\nu_3(\text{NO}_3)$ ). The bands at 1647 and 1620, 1581 and 1545, and 1310 and 1270 cm<sup>-1</sup> correspond to bridging nitrates, bidentate nitrates, and monodentate nitrates, respectively.<sup>55-58, 65, 66</sup> Bands around 1680 cm<sup>-1</sup> are not well established in the literature, but evolve in parallel with bridge nitrates, suggesting they are an additional bridging species (e.g. metal-support bridging nitrates). Additional smaller peaks near 1200 cm<sup>-1</sup> may contribute to the broad band from 1350 to 1200 cm<sup>-1</sup> due to  $\nu_3$  splitting of the bridge ( $\Delta\nu_3 \sim 420$  cm<sup>-1</sup>) and bidentate ( $\Delta\nu_3 \sim 300$  cm<sup>-1</sup>) species. The band at 1488 cm<sup>-1</sup> has been previously seen in the literature, but doesn't have a clear assignment;<sup>61, 66</sup> it can be a chelating nitrate or hydrogenated NO species such as NH<sub>2</sub>NO, but unlikely to be ammonia species due to the lack of more intense bands at 1434 cm<sup>-1</sup>.

On TiO<sub>2</sub> and V<sub>2</sub>O<sub>5</sub> supports, it is generally understood that nitrates form via surface hydroxides and are the primary contributors towards the negative bands at 3500 to 3800 and 2047 cm<sup>-1</sup>,<sup>57, 58, 65</sup> following the reaction,



where [O] is surface oxygen, of which vanadium is a source. These previous reports are further substantiated by the band intensities of nitrates decreasing and approaching zero in concert with the those of OH and V<sup>5+</sup>=O with increasing temperature (Figure 4a). Among all the nitrate species, the bidentate nitrates at 1581 and 1545 cm<sup>-1</sup> are the most stable and are still present in small amounts at 300 °C. The conditions under which nitrates are stable appear to be opposite for nitrosyl adsorption on Pd, as the bands between 1725 and 1900 cm<sup>-1</sup> remained relatively weak until the nitrate bands diminished at 175 °C. At the point when nitrate bands become less intense than Pd-NO nitrosyls, Pd begins to reduce NOx species, supported by the disappearance of NO<sup>+</sup> bands and the gradual increase in Pd oxidation state as measured by XAS (cf. Figure S3e). Here it can be inferred that at lower temperatures, NOx is more easily oxidized by the support and PdO, leading to more oxidized nitrogen species. As temperature increases, nitrates at the metal-support interface become reduced by Pd





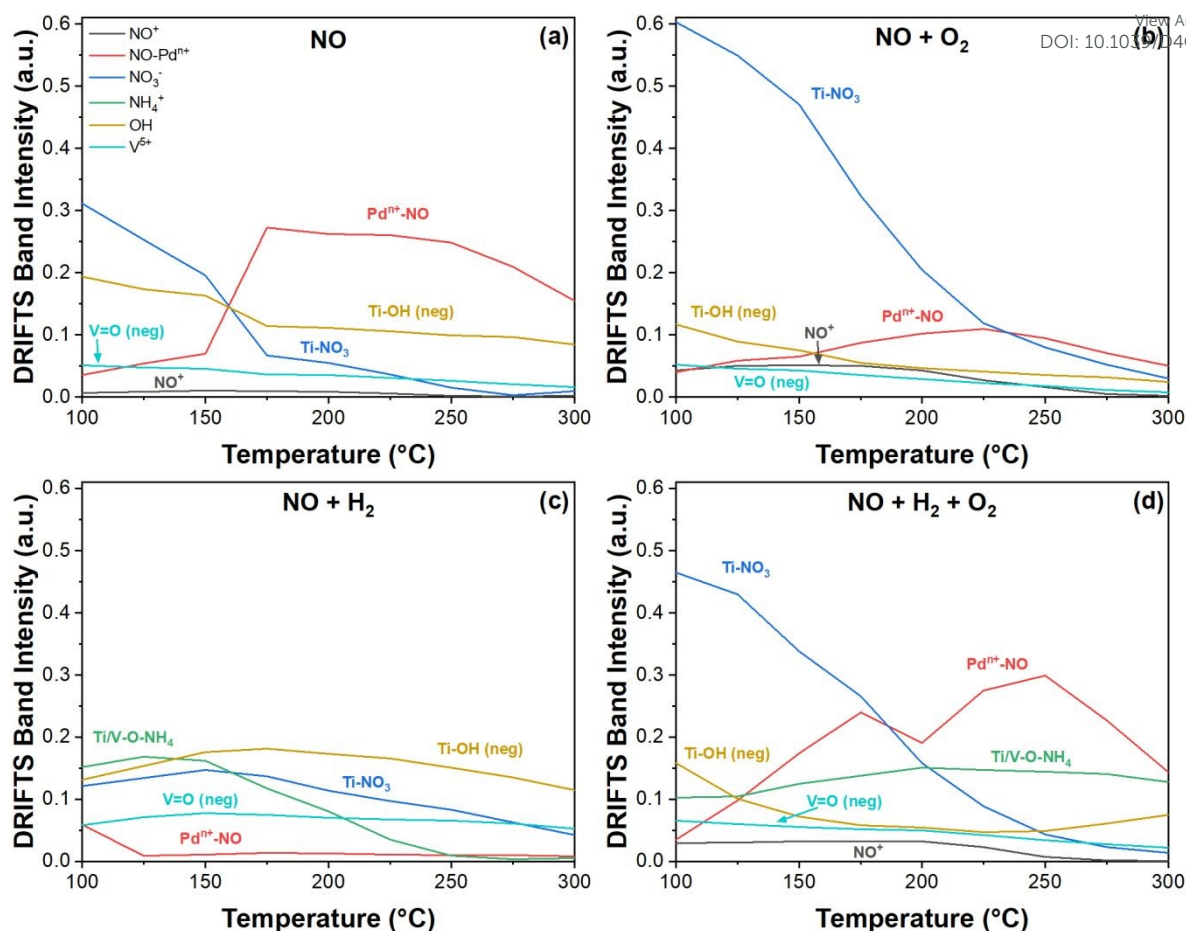


**Fig. 4** Absolute intensities of selected IR bands of reactive intermediates from DRIFTS pseudo-absorbance spectra for (a) NO, (b) NO and O<sub>2</sub>, (c) NO and H<sub>2</sub>, and (d) SCR gas mixtures. The V<sup>5+</sup> and OH bands are negative in absorbance and represent the relative decrease in V=O and Ti-OH species, respectively.

and form Pd<sup>n+</sup>-NO nitrosyl species. These findings are observed to a greater extent with other gas conditions below.

**Co-adsorption of NO and O<sub>2</sub>.** Introduction of O<sub>2</sub> into the gas feed largely leaves the NO adsorption spectra unchanged (Figure 5), with mostly changes in band intensity; the chemistry corresponding with OH bands, V<sup>5+</sup> and NO<sup>+</sup> bands, and nitrate bands largely remain the same as with the NO condition. The addition of O<sub>2</sub> only leads to increased nitrate presence by oxidizing NO and makes the 1620 cm<sup>-1</sup> bands more stable at higher temperatures as shown in Figure 5b. The 1488 cm<sup>-1</sup> band disappears and the 1310 cm<sup>-1</sup> band redshifts to 1290 cm<sup>-1</sup> as a lower frequency monodentate nitrate. Bidentate nitrates remain the most stable nitrate species and are the only nitrates remaining above 250 °C.

The most significant changes can be seen in the nitrosyl bands from 1725 to 1900 cm<sup>-1</sup>, where the main similarity between the NO and NO + O<sub>2</sub> conditions is the desorption of NO from Pd above 250 °C. In the co-adsorption of NO and O<sub>2</sub>, the splitting among bands at 1826 and 1813 cm<sup>-1</sup> is more pronounced, and a new band emerges at 1796 cm<sup>-1</sup>. These bands, as well as the 1776 cm<sup>-1</sup> band, evolve in unison, increasing until 225 °C before gradually decaying with increasing temperature due to rapid desorption of NO from Pd.

The maximum intensity of these bands is substantially less than with the adsorption of only NO. Also unlike in the previous gas condition, Pd gradually reduces with increasing temperature during the co-adsorption of NO and O<sub>2</sub>, as shown by XAS (cf. Figure S3b), which correlates both with Pd-NO gradually increasing and a substantial presence of NO<sup>+</sup> from broad and intense bands at 2181 cm<sup>-1</sup>. The oxidation state of Pd levels out and remains constant at 225 °C, at which point Pd-NO and NO<sup>+</sup> bands decrease.

From the combined observations of NO adsorption and NO and O<sub>2</sub> co-adsorption, it can be inferred that nitrosyl species on Pd form more easily from nitrates which are reduced by Pd, given the stronger Pd<sup>n+</sup>-NO bands with NO alone. The slight reduction of PdO observed with the co-adsorption of NO and O<sub>2</sub> suggests that PdO is able to some degree oxidize and store NOx. However, given the more significant oxidation of Pd and greater presence of nitrosyl species on Pd, as observed during NO adsorption, it appears Pd more efficiently reduces surface NOx.

**Co-adsorption of NO and H<sub>2</sub>.** The introduction of a strong reducing agent drastically changes the species observed in DRIFTS measurements. While most of the species described above are present to some degree, with exception to the bidentate nitrates which are almost fully absent except for a



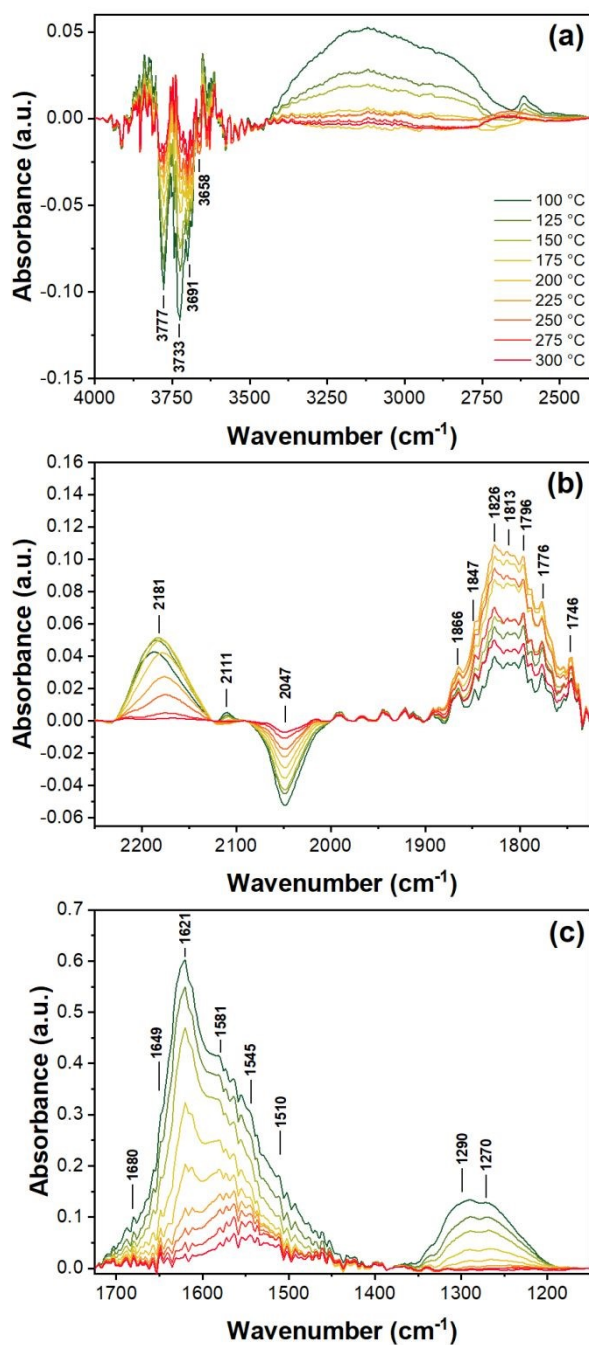


**Figure 5.** Temperature dependent DRIFTS spectra of the 1%Pd/5%V<sub>2</sub>O<sub>5</sub>/20%TiO<sub>2</sub>-Al<sub>2</sub>O<sub>3</sub> catalyst under a flow of 1000 ppm NO and 10% O<sub>2</sub> in Ar, shown at (a) high wavenumbers for OH (negative) and water bands, (b) middle wavenumbers for NO<sup>+</sup>, V=O (negative), and Pd-NO bands, and (c) low wavenumbers for support nitrate and nitrite bands.

weak band at 1578 cm<sup>-1</sup>, several new peaks appear at 3336, 3249, 3174, 3033, and 2800 cm<sup>-1</sup> (Figure 6a), 1890 cm<sup>-1</sup> (Figure 6b), and 1512, 1454, 1433, 1402, 1333, and 1235 cm<sup>-1</sup> (Figure 6c).

The bridging nitrate species are present at all measured temperatures, and the bands decrease slightly with increasing

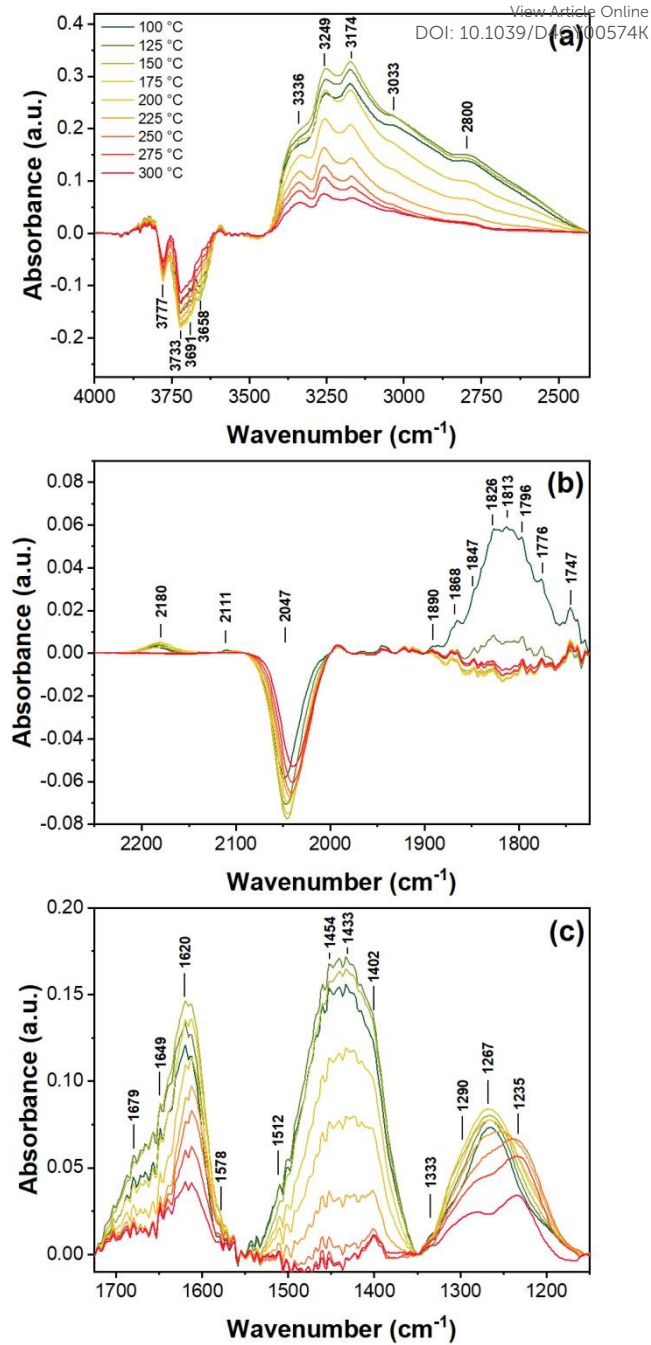


**Figure 6.** Temperature dependent DRIFTS spectra of the 1%Pd/5%V<sub>2</sub>O<sub>5</sub>/20%TiO<sub>2</sub>-Al<sub>2</sub>O<sub>3</sub> catalyst under a flow of 1000 ppm NO and 5000 ppm H<sub>2</sub> in Ar, shown at (a) high wavenumbers for OH (negative), ammonia, and water bands, (b) middle wavenumbers for NO<sup>+</sup>, V=O (negative), and Pd-NO bands, and (c) low wavenumbers for support nitrates, nitrites, and ammonia bands.

temperature, matching well with the negative OH and V<sup>5+</sup> bands. Despite the apparent stability of nitrate species under reducing conditions, the overall intensities of these bands are substantially less than during the co-adsorption of NO and O<sub>2</sub>. Additionally, the lower wavenumber bidentate nitrate species are largely absent at all temperatures, indicating their relative instability under reducing conditions. Signs of altered nitrate



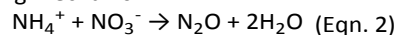
chemistry are given by the blueshift of the OH bands and redshift of the  $V^{5+}$  bands with increasing temperature. An additional sign of altered chemistry is the presence of a monodentate nitrite band  $\nu_3(\text{NO}_2)$  at  $1512\text{ cm}^{-1}$ , which is relatively weak and rapidly vanishes with increasing temperature.

Unlike the previously discussed gas conditions, the  $\text{Pd}^{\text{n+}}\text{-NO}$  band at  $1813\text{ cm}^{-1}$  was observed at  $100\text{ }^\circ\text{C}$  and rapidly vanished by  $150\text{ }^\circ\text{C}$ , along with neighboring and less intense  $\text{Pd}^{2+}$ ,  $\text{Pd}^+$ , and  $\text{Pd}^0$  bands at  $1868$ ,  $1776$ , and  $1747\text{ cm}^{-1}$ , respectively, (Figure 6b). The pathway through which NO adsorbs onto Pd under these reducing conditions at these temperatures is not clear, as both the average oxidation state of Pd (Figure 1c) and nitrosyl bands (Figure 4c) decrease simultaneously, but the overall lack of  $\text{NO}^+$  and low presence of nitrates suggests that NO is more likely reduced while adsorbing onto Pd. Additionally, the presence of  $\text{H}_2$  without  $\text{O}_2$  causes these linearly adsorbed species to be highly unstable and are likely converted into ammonia species, explained in more detail below.

New peaks from  $2500$  to  $3500\text{ cm}^{-1}$  and  $1350$  to  $1500\text{ cm}^{-1}$  are all associated with the formation of ammonium ions ( $\text{NH}_4^+$ ) on Brønsted acid sites and  $\text{NH}_3$  adsorbed on Lewis acid sites. It is well reported in the literature that the  $3358$  and  $3240\text{ cm}^{-1}$  bands belong to the  $\nu_3(\text{N-H})$  modes, of  $\text{NH}_3$  on Lewis sites, whereas the  $3183$ ,  $3033$ , and  $2800\text{ cm}^{-1}$  bands are for the  $\nu_{\text{as}}(\text{N-H})$ ,  $\nu_{\text{as}}(\text{N-H})$ , and  $2\delta_{\text{as}}(\text{H-N-H})$  modes, respectively, of  $\text{NH}_4^+$  adsorbed on Brønsted acid sites.<sup>57, 60, 66, 67</sup> Lower frequency  $\text{NH}_4^+$   $\delta_{\text{as}}(\text{H-N-H})$  modes are found at  $1454$ ,  $1433$ , and  $1402\text{ cm}^{-1}$ ,<sup>67</sup> with a corresponding  $\delta_s(\text{H-N-H})$  mode at  $1660\text{ cm}^{-1}$ .<sup>33</sup> Low frequency modes of  $\text{NH}_3$  adsorbed on Lewis acid sites, which overlap with the bands of monodentate nitrates at  $1297$ ,  $1282$ , and  $1256\text{ cm}^{-1}$ , are particularly difficult to isolate but may contribute to band broadening near  $1300\text{ cm}^{-1}$ . A weak band at  $1333\text{ cm}^{-1}$  is observed with questionable significance and may be attributed to nitro-compounds or N-N vibrations of  $\text{cis-N}_2\text{O}_2$  species.<sup>58</sup> In the case of nitro-compounds, an additional band at  $1580\text{ cm}^{-1}$  would be expected, but overlaps significantly with nitrate species.  $\text{N}_2\text{O}_2$  species would have counterpart bands below  $1050\text{ cm}^{-1}$  which is below the sample cut-off. During the co-adsorption of NO and  $\text{H}_2$ , this band is of questionable value but becomes more significant under SCR conditions, as discussed in detail below, suggesting it belongs to features of partially reduced NOx species which are not observed in the absence of  $\text{H}_2$ .

$\text{NH}_4^+$  adsorbed on Brønsted acid sites remain stable until around  $200\text{ }^\circ\text{C}$ , where they decay following the rapid reduction of Pd, as shown in Figures 1c and 4c. By  $250\text{ }^\circ\text{C}$ , Pd is fully reduced and negligible  $\text{NH}_4^+$  remains on Brønsted acid sites. Beyond  $250\text{ }^\circ\text{C}$  and when NO approaches full conversion, only the bands at  $1402$ ,  $3174$ ,  $3249$ , and  $3336\text{ cm}^{-1}$  remain. The more intense modes of  $\text{NH}_3$  adsorbed on Lewis acid sites suggest these as the dominant surface ammonia species. The decay curve of  $\text{NH}_4^+$  species matches that of  $\text{N}_2\text{O}$  in Figure 1a, suggesting that  $\text{NH}_4^+$  is a critical intermediate for the formation of  $\text{N}_2\text{O}$ . The dependence of ammonium ions on oxidized Pd suggest  $\text{NH}_4^+$  forms at the metal-support interface via the reduction of NOx species bridging PdO and  $\text{TiO}_2$  Brønsted acid

sites with activated hydrogen. These interfacial  $\text{NH}_4^+$  are then able to react with nitrates bridging PdO and  $\text{TiO}_2$ , forming  $\text{N}_2\text{O}$  via the following mechanism:<sup>68</sup>



Once bulk reduced Pd appears (cf. Figure 1c), ammonium ions are unable to form – as indicated by the disappearance of  $\text{NH}_4^+$  ( $1433\text{ cm}^{-1}$ ) bands (cf. Figure 4c, Figure 6c) – and activated hydrogen becomes the dominant reducing agent, fully reducing nitrosyls and nitrates to  $\text{N}_2$  and  $\text{H}_2\text{O}$  and eliminating  $\text{N}_2\text{O}$  as a product. Also under these conditions, trace amounts of  $\text{N}_2\text{O}$  in the gas phase are easily converted.

$\text{NH}_3$  adsorbed on Lewis acid sites becomes the dominant ammonia species at high temperatures, as indicated by lingering bands at  $3249$  and  $3336\text{ cm}^{-1}$ . This suggests that Lewis acid sites on the support are not significantly impacted by the state of Pd and that  $\text{NH}_3$  is a more stable reactive intermediate than  $\text{NH}_4^+$  at high temperatures. No significant gaseous  $\text{NH}_3$  was detected in the MS data ( $m/z = 15$ ), which could indicate that  $\text{NH}_3$  adsorbed at Lewis acid sites on the titania-vanadia support performs SCR of NOx in parallel with activated  $\text{H}_2$  on Pd, matching previous reports;<sup>28</sup> however, this cannot be confidently concluded due to limitations in measuring small quantities of nitrogen species, especially in the case of  $\text{NH}_3$ , which has only a minor fragmentation ion at  $m/z = 15$ .

***In-Situ* DRIFTS of the  $\text{H}_2$ -SCR of NO.** With the addition of oxygen to the NO/ $\text{H}_2$  mixture, which results in typical SCR conditions, no new bands appeared in DRIFTS spectra (Figure 7). However, the temperature evolution of active metal-NO, ammonia, and nitrate modes are distinct, and aspects of each condition are visible and help elucidate the complex chemistry observed. The temperature dependence of bridge nitrates ( $1620\text{ cm}^{-1}$ ), Pd-NO ( $1813\text{ cm}^{-1}$ ),  $\text{NO}^+$  ( $2182\text{ cm}^{-1}$ ), OH<sup>-</sup> ( $3733\text{ cm}^{-1}$ ),  $V^{5+}$  ( $2047\text{ cm}^{-1}$ ),  $\text{NH}_4^+$  ( $1427\text{ cm}^{-1}$ ), and  $\text{NH}_3$  ( $1385\text{ cm}^{-1}$ ) IR modes are shown in Figure 4d and contrast with the other gas conditions in Figures 4a-c.

Similar to the observations of the previously discussed gas mixtures (cf. Figure 4), the negative OH and  $V^{5+}$  bands decrease in absolute area alongside the bridge nitrate bands with increasing temperature. However, the competition between  $\text{NH}_4^+$  and nitrates for adsorbing on Brønsted acid sites is more pronounced; from  $50$  to  $100\text{ }^\circ\text{C}$ , where  $\text{NH}_4^+$  species ( $1427\text{ cm}^{-1}$ ) are most prevalent, the bridge and bidentate nitrate bands are less intense and grow in intensity from  $125\text{ }^\circ\text{C}$  as adsorbed  $\text{NH}_4^+$  decreases in prevalence. Additionally, the  $1620\text{ cm}^{-1}$  bridge species undergoes a slight blueshift in the presence of  $\text{NH}_4^+$  at  $50$  and  $75\text{ }^\circ\text{C}$ . The clash between these molecules further suggests that bridge and bidentate nitrates form at Brønsted acid sites and compete with  $\text{NH}_4^+$ . In the absence of  $\text{O}_2$ ,  $\text{NH}_4^+$  species dominate at low temperatures. The presence of  $\text{O}_2$  does not appear to lower the stability of  $\text{NH}_4^+$  species, considering that the band intensities at  $1427$  and  $3031\text{ cm}^{-1}$  are equal or higher than observed with just the NO +  $\text{H}_2$  condition.  $\text{O}_2$  rather promotes the formation of nitrates and causes the low frequency bands of  $\text{NH}_4^+$  adsorbed on Brønsted acid sites to redshift with increasing temperature. It is important to note that the presence of  $\text{O}_2$  also promotes  $\text{NH}_4^+$  species at higher temperatures. Under the NO +  $\text{H}_2$  condition,  $\text{NH}_4^+$  species nearly



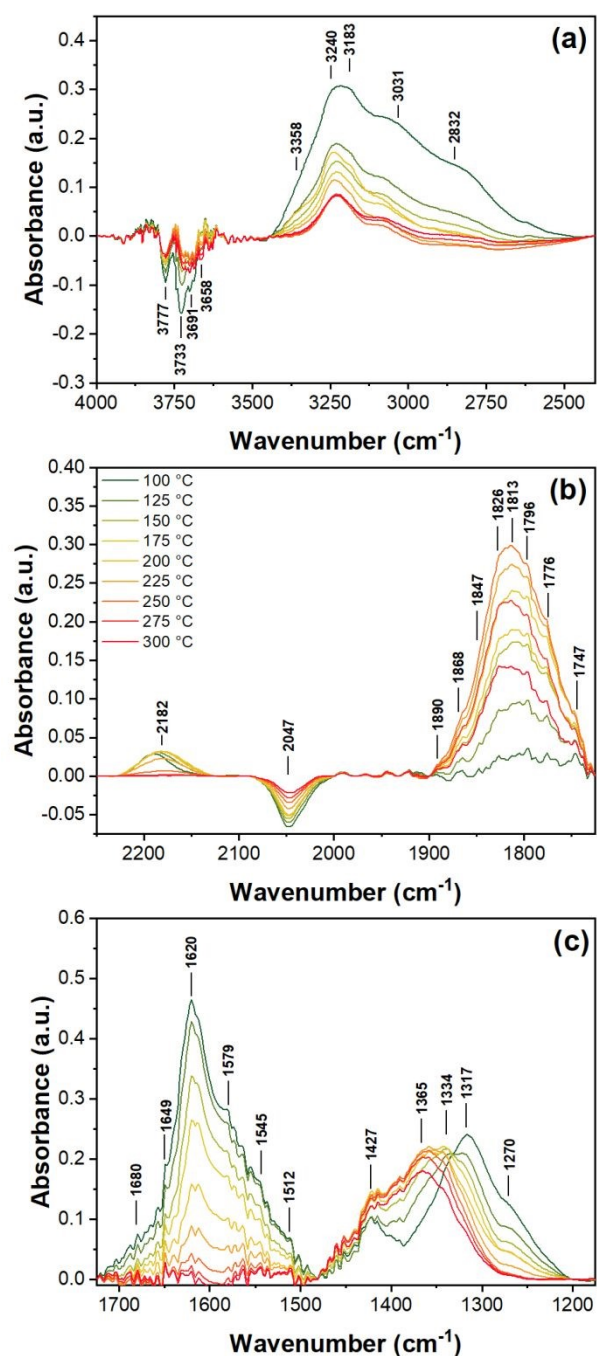


**Figure 7.** Temperature dependent DRIFTS spectra of the 1%Pd/5%V<sub>2</sub>O<sub>5</sub>/20%TiO<sub>2</sub>-Al<sub>2</sub>O<sub>3</sub> catalyst under a flow of 1000 ppm NO, 5000 ppm H<sub>2</sub>, and 10% O<sub>2</sub> in Ar, shown at (a) high wavenumbers for OH (negative), ammonia, and water bands, (b) middle wavenumbers for NO<sup>+</sup>, V=O (negative), and Pd-NO bands, and (c) low wavenumbers for support nitrates, nitrites, and ammonia bands.

fully diminished by 275 °C, whereas the low frequency NH<sub>4</sub><sup>+</sup> band at 1427 cm<sup>-1</sup> remains present in significant amounts at 300 °C with the addition of O<sub>2</sub>. No significant change was observed in the MS intensity of N<sub>2</sub>O which suggests O<sub>2</sub> limits the conversion of NH<sub>x</sub> species to N<sub>2</sub>O. However, the small amounts

of N<sub>2</sub>O expected from this catalyst (i.e. 50 ppm)<sup>34</sup> during SCR of NOx was not detected by MS. DOI: 10.1039/D4CY00574K

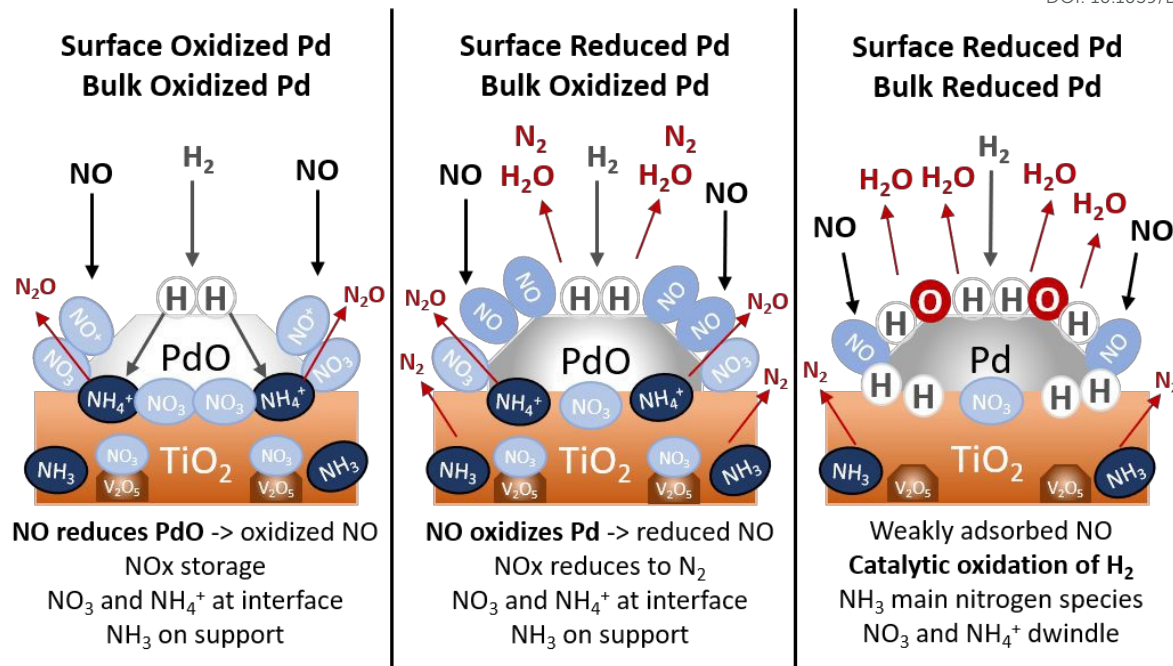
Another significant change due to the addition of O<sub>2</sub> to the NO + H<sub>2</sub> mixture is the more significant presence of bands between 1300 and 1400 cm<sup>-1</sup>, which undergo a blueshift with increasing temperatures. From the band at 1317 cm<sup>-1</sup>, generally assigned to monodentate nitrates on TiO<sub>2</sub>, is significant at 50 °C but gradually decreases and seemingly shifts to 1334 cm<sup>-1</sup> at 175 °C and ultimately 1365 cm<sup>-1</sup> by 300 °C. Part of this shift can be explained by diminishing nitrate bands throughout the entire spectrum. However, the blueshift to frequencies closer to 1365 cm<sup>-1</sup> correlates with the onset of SCR activity at 200 °C (Figure 1b), and all bands around 1365 cm<sup>-1</sup> begin to decrease in intensity as NO conversion decreases beyond 250 °C. Here it can be inferred that more complex partially reduced N<sub>x</sub>O<sub>y</sub> species (e.g. nitro-compounds)<sup>55, 58</sup> are formed as SCR intermediates.

The bands for active metals from 1725 and 1900 cm<sup>-1</sup> indicate/support three temperature regimes relevant for the performance of the H<sub>2</sub>-SCR reaction. Similar to the NO and NO + O<sub>2</sub> conditions, the Pd-NO bands are largely absent until the bridge nitrate species at 1649 and 1620 cm<sup>-1</sup> significantly decrease. In this low temperature regime, below 200 °C and the onset of SCR activity, the abundance of nitrates and NO<sup>+</sup> species suggests that NO is more favorably oxidized. Given the gradual reduction of Pd, as shown by XANES in Figure 1d and as observed during the co-adsorption of NO and O<sub>2</sub>, PdO appears able to oxidize NO<sub>x</sub> and form metal-support bridge nitrates (1680 cm<sup>-1</sup>) according to Equation 1. This then is an intermediate step towards the formation of Pd-NO nitrosyls. After the onset of SCR activity above 200 °C, nitrates and NO<sup>+</sup> species diminish, converting to nitrosyl species on Pd and forming PdO, as observed in the adsorption of NO alone. Above 250 °C, SCR activity decreases in intensity, Pd-NO IR bands rapidly shrink, and the average oxidation state of Pd begins to significantly decline. Here, as observed with the adsorption of NO and the co-adsorption of NO and O<sub>2</sub>, the rate of desorption of NO limits the presence of NO species on the active metal. In turn, activated hydrogen on bulk reduced Pd more readily reduces Pd and combusts with impinging O<sub>2</sub>.

It is notable that the conversion of NO decreases less drastically as the desorption of NO from Pd and the reduction of Pd. This can be explained by the role of the titania-vanadia support, which has been previously shown to reduce NO<sub>x</sub> at high temperatures without the presence of active metal.<sup>26</sup> To this end, NH<sub>3</sub> adsorbed on Lewis acid sites, indicated by the persistent band at 3240 cm<sup>-1</sup>, is a species which exists independently of the state of Pd which is efficient at reducing NO<sub>x</sub> stored on the TiO<sub>2</sub> support during H<sub>2</sub>-SCR.<sup>28</sup>

These findings point towards Pd<sup>n+</sup>-NO as the active surface intermediate for H<sub>2</sub>-SCR activity on the active metal and NH<sub>3</sub> adsorbed onto Lewis acid sites as an active intermediate for SCR on the support. Notably, at 250 °C where NO conversion is maximized, the nitrosyl (1796, 1813, and 1826 cm<sup>-1</sup>) bands are also at their maximum intensity. When the temperature increases, NO conversion weakens and Pd becomes more reduced due to runaway activation of H<sub>2</sub> and its subsequent catalytic oxidation, which correlates with the decrease in the



Scheme 1. Evolution of nitrogen species on Pd/V<sub>2</sub>O<sub>5</sub>/TiO<sub>2</sub>-Al<sub>2</sub>O<sub>3</sub> with respect to Pd oxidation stateView Article Online  
DOI: 10.1039/D4CY00574K

area of all three IR bands. Despite the rapid reduction of Pd, the presence of O<sub>2</sub> slows this reduction relative to what was observed during the co-adsorption of NO and H<sub>2</sub>. This suggests that O<sub>2</sub> buffers the Pd state during SCR, delaying and limiting the rate of reduction.

## Conclusions

The average oxidation state of Pd on a 1%Pd/5%V<sub>2</sub>O<sub>5</sub>/20%TiO<sub>2</sub>-Al<sub>2</sub>O<sub>3</sub> catalyst create three distinct regimes and plays a pivotal role in which adsorbed species exist on the surface and which reaction pathways for NO<sub>x</sub> reduction occur during H<sub>2</sub>-SCR (cf. Scheme 1). The prevalence of PdO on the surface and in the bulk material, mediated by the presence of O<sub>2</sub>, influence how NO<sub>x</sub> is stored and reacts with adsorbed reducing agents.

In the case of mostly oxidized Pd, where both the surface and bulk are PdO-like, gradual reduction of Pd was observed during adsorption of NO, both with and without O<sub>2</sub>. This coincided with the formation of NO<sup>+</sup> ions and nitrates, demonstrating that NO is able to reduce PdO. While Pd<sup>n+</sup>-NO adsorbates were observed under these conditions, oxidation of NO favors the formation of other nitrogen species (e.g. nitrates, nitrites, nitro-compounds) which store at the metal-support interface or on the metal oxide. Highly oxidized Pd is not directly conducive to SCR, either due to stable NO<sub>x</sub> adsorbates in the presence of O<sub>2</sub> or due to the formation of undesired N<sub>2</sub>O from the combination of NH<sub>4</sub><sup>+</sup> and nitrates at the metal-support interfacial Brønsted acid sites.

The SCR of NO is most efficient on slightly reduced Pd, in which the surface contains a significant amount of Pd<sup>0</sup> for NO<sub>x</sub> adsorbates to oxidize. Metal-support bridged nitrates react with Pd<sup>0</sup> to form adsorbed Pd<sup>n+</sup>-NO. H<sub>2</sub> then further reduces these nitrosyl species to H<sub>2</sub>O and N<sub>2</sub>. Partially reduced adsorbed

N<sub>x</sub>O<sub>y</sub> species (e.g. nitro-compounds) are also present in significant amounts under SCR conditions when Pd is also partially reduced.

Once bulk PdO is reduced to metallic Pd, both O<sub>2</sub> and H<sub>2</sub> activate and catalytic oxidation of H<sub>2</sub> becomes the favored reaction pathway. At temperatures above 250 °C, the fast desorption of NO from Pd outpaces the ability for nitrates to oxidize Pd, further inhibiting SCR activity and causing a runaway reduction of Pd.

Ammonium ions adsorbed on Brønsted acid sites at the Pd-support interface, are highly affected by the Pd oxidation state. In the absence of O<sub>2</sub>, NH<sub>4</sub><sup>+</sup> ions are not formed on reduced Pd. The presence of O<sub>2</sub> stabilizes adsorbed ammonium and restricts the undesired conversion to N<sub>2</sub>O. NH<sub>3</sub> adsorbed on Lewis acid sites exists independent of the Pd state, with or without O<sub>2</sub>.

Here the vanadia-titania support plays a critical role in the SCR of NO by oxidizing impinging NO and storing it on the surface as stable nitrates and nitrites at Brønsted acid sites. V=O readily oxidizes NO across all measured temperatures both in the presence and absence of O<sub>2</sub>. The Lewis acid sites on TiO<sub>2</sub> also permit stable NH<sub>3</sub> formation in the presence of H<sub>2</sub>, which selectively reduce adsorbed NO<sub>x</sub> to N<sub>2</sub> at high temperatures when NO desorbs from the active metal.

From the data presented herein, in order to optimize SCR of NO<sub>x</sub> by H<sub>2</sub>, metal-support bridge nitrates need to be the focus as they are a form of NO<sub>x</sub> storage as well as a critical intermediate for nitrosyls on the active metal. This would require increased Brønsted acid site prevalence near or at the active metal interface. However, it should be kept in mind that these sites are susceptible to NH<sub>4</sub><sup>+</sup> ions and N<sub>2</sub>O formation especially under rich exhaust conditions. With sufficient O<sub>2</sub>, the sites will ultimately increase the amount of desired reactive intermediates and therefore increase catalytic activity.



## Author Contributions

Thomas Eldridge: writing – original draft, visualization, validation, data curation, methodology, investigation. Michael Borchers: methodology, investigation. Patrick Lott: writing – review & editing. Jan-Dierk Grunwaldt: writing – review & editing, funding acquisition, resources, supervision. Dmitry Doronkin: writing – review & editing, validation, methodology, investigation, supervision

## Conflicts of interest

There are no conflicts to declare.

## Acknowledgements

The work has been supported by the Helmholtz Association through the MTET (Materials and Technologies for Energy Transition) program.

We acknowledge DESY (Hamburg, Germany), a member of the Helmholtz Association HGF, for the provision of experimental facilities. Parts of this research were carried out at PETRA III and we would like to thank Dr. Aleksandr Kalinko and Dr. Wolfgang Caliebe for assistance in using beamline P64. Beamtime was allocated for proposal I-20220246.

We thank Dr. Olaf Deutschmann for provision of infrastructure, resources, and fruitful discussion.

## References

1. G. Ertl, H. Knözinger and J. Weitkamp, *Handbook of heterogeneous catalysis*, VCH Weinheim, 1997.
2. K. F. Kalz, R. Kraehnert, M. Dvoyashkin, R. Dittmeyer, R. Gläser, U. Krewer, K. Reuter and J.-D. Grunwaldt, *ChemCatChem*, 2017, **9**, 17-29.
3. C. M. White, R. R. Steeper and A. E. Lutz, *International Journal of Hydrogen Energy*, 2006, **31**, 1292-1305.
4. S. Verhelst, P. Maesschalck, N. Rombaut and R. Sierens, *International Journal of Hydrogen Energy*, 2009, **34**, 4406-4412.
5. R. Jeeragal and K. A. Subramanian, *Journal of Thermal Science*, 2019, **28**, 789-800.
6. K. W. Scholl and S. C. Sorenson, *SAE Transactions*, 1993, 1450-1462.
7. I. Nova, C. Ciardelli, E. Tronconi, D. Chatterjee and B. Bandl-Konrad, *Catal Today*, 2006, **114**, 3-12.
8. A. Grossale, I. Nova, E. Tronconi, D. Chatterjee and M. Weibel, *J Catal*, 2008, **256**, 312-322.
9. M. Colombo, I. Nova and E. Tronconi, *Catal Today*, 2012, **197**, 243-255.
10. T. Günter, H. W. Carvalho, D. E. Doronkin, T. Sheppard, P. Glatzel, A. J. Atkins, J. Rudolph, C. R. Jacob, M. Casapu and J.-D. Grunwaldt, *Chem Commun*, 2015, **51**, 9227-9230.
11. O. Deutschmann and J.-D. Grunwaldt, *Chemie Ingenieur Technik*, 2013, **85**, 595-617.
12. A. Boubnov, H. W. P. Carvalho, D. E. Doronkin, T. Günter, E. Gallo, A. J. Atkins, C. R. Jacob and J.-D. Grunwaldt, *J Am Chem Soc*, 2014, **136**, 13006-13015.
13. Y. Ganjkanlou, T. V. W. Janssens, P. N. R. Venneström, L. Mino, M. C. Paganini, M. Signorile, S. Bordiga and G. Berlier, *Applied Catalysis B: Environmental*, 2020, **278**, 119337.
14. Z. Liu, J. Wu and C. Hardacre, *Catalysis Surveys from Asia*, 2018, **22**, 146-155.
15. Z. Hu and R. T. Yang, *Industrial & Engineering Chemistry Research*, 2019, **58**, 10140-10153.
16. J.-D. Grunwaldt, N. v. Vegten and A. Baiker, *Chem Commun*, 2007, DOI: 10.1039/B710222D, 4635-4637.
17. E. K. Dann, E. K. Gibson, R. H. Blackmore, C. R. A. Catlow, P. Collier, A. Chutia, T. E. Erden, C. Hardacre, A. Kroner, M. Nachtegaal, A. Raj, S. M. Rogers, S. F. R. Taylor, P. Thompson, G. F. Tierney, C. D. Zeinalipour-Yazdi, A. Goguet and P. P. Wells, *Nature Catalysis*, 2019, **2**, 157-163.
18. C. N. Costa and A. M. Efstathiou, *Environmental Chemistry Letters*, 2004, **2**, 55-58.
19. C. N. Costa and A. M. Efstathiou, *The Journal of Physical Chemistry B*, 2004, **108**, 2620-2630.
20. C. N. Costa and A. M. Efstathiou, *Applied Catalysis B: Environmental*, 2007, **72**, 240-252.
21. G. G. Olympiou and A. M. Efstathiou, *Chem Eng J*, 2011, **170**, 424-432.
22. P. Wu, L. Li, Q. Yu, G. Wu and N. Guan, *Catal Today*, 2010, **158**, 228-234.
23. D. T. Koch, E. Eßer, S. Kureti and A. Sousa, *MTZ - Motortechnische Zeitschrift*, 2020, **81**, 32-39.
24. B. Wen, *Fuel*, 2002, **81**, 1841-1846.
25. G. Qi, R. T. Yang and L. T. Thompson, *Applied Catalysis A: General*, 2004, **259**, 261-267.
26. G. Qi, R. T. Yang and F. C. Rinaldi, *J Catal*, 2006, **237**, 381-392.
27. L. Wang, C. Yin and R. T. Yang, *Applied Catalysis A: General*, 2016, **514**, 35-42.
28. Z. Hu, X. Yong, D. Li and R. T. Yang, *J Catal*, 2020, **381**, 204-214.
29. V. K. Patel and S. Sharma, *Catal Today*, 2021, **375**, 591-600.
30. A. Ueda, T. Nakao, M. Azuma and T. Kobayashi, *Catal Today*, 1998, **45**, 135-138.
31. R. Burch and M. D. Coleman, *Applied Catalysis B: Environmental*, 1999, **23**, 115-121.
32. K. Duan, Z. Wang, C. Hardacre, Z. Liu, S. Chansai and C. Stere, *Catal Today*, 2019, **332**, 69-75.
33. N. Macleod and R. M. Lambert, *Catal Lett*, 2003, **90**, 111-115.
34. M. Borchers, K. Keller, P. Lott and O. Deutschmann, *Industrial & Engineering Chemistry Research*, 2021, **60**, 6613-6626.
35. F. J. P. Schott, P. Balle, J. Adler and S. Kureti, *Applied Catalysis B: Environmental*, 2009, **87**, 18-29.
36. M. Leicht, F. J. P. Schott, M. Bruns and S. Kureti, *Applied Catalysis B: Environmental*, 2012, **117-118**, 275-282.
37. C. Hahn, M. Endisch, F. J. P. Schott and S. Kureti, *Applied Catalysis B: Environmental*, 2015, **168-169**, 429-440.
38. C. Hahn, M. Endisch and S. Kureti, *Top Catal*, 2017, **60**, 238-242.
39. T. Nanba, C. Kohno, S. Masukawa, J. Uchisawa, N. Nakayama and A. Obuchi, *Applied Catalysis B: Environmental*, 2003, **46**, 353-364.



40. H. Hamada and M. Haneda, *Applied Catalysis A: General*, 2012, **421-422**, 1-13.
41. Z. Hong, X. Sun, Z. Wang, G. Zhao, X. Li and Z. Zhu, *Catal. Sci. Technol.*, 2019, **9**, 3994-4001.
42. M. Borchers, P. Lott and O. Deutschmann, *Top Catal*, 2023, **66**, 973-984.
43. L. Zhang, Y. Shan, Z. Yan, Z. Liu, Y. Yu and H. He, *Journal of Environmental Sciences*, 2024, **138**, 102-111.
44. H. Topsøe, *J Catal*, 2003, **216**, 155-164.
45. A. Urakawa, N. Maeda and A. Baiker, *Angewandte Chemie-International Edition*, 2008, **47**, 9256-9259.
46. L. van Beek, D. Jain, P. Gholkar, T. J. Eldridge, H. P. Nguyen, K. Muramoto and A. Urakawa, *Catal Today*, 2024, **429**, 114466.
47. A. M. Gänzler, M. Casapu, D. E. Doronkin, F. Maurer, P. Lott, P. Glatzel, M. Votsmeier, O. Deutschmann and J.-D. Grunwaldt, *The Journal of Physical Chemistry Letters*, 2019, **10**, 7698-7705.
48. B. Bornmann, J. Kläs, O. Müller, D. Lützenkirchen-Hecht and R. Frahm, *AIP Conference Proceedings*, 2019, **2054**, 040008.
49. D. E. Doronkin, H. Lichtenberg and J.-D. Grunwaldt, *XAFS Techniques for Catalysts, Nanomaterials, and Surfaces*, 2017, 75-89.
50. D. Lützenkirchen-Hecht, J.-D. Grunwaldt, M. Richwin, B. Griesebock, A. Baiker and R. Frahm, *Physica Scripta*, 2005, **2005**, 831.
51. M. Newville, *Larch: an analysis package for XAFS and related spectroscopies*, *Journal of Physics: Conference Series*, 2013.
52. B. Ravel and M. Newville, *J. Synchrot. Radiat.*, 2005, **12**, 537-541.
53. A. Puig-Molina, F. M. Cano and T. V. W. Janssens, *The Journal of Physical Chemistry C*, 2010, **114**, 15410-15416.
54. M. Kantcheva, *J Catal*, 2001, **204**, 479-494.
55. J. M. Watson and U. S. Ozkan, *J Catal*, 2002, **210**, 295-312.
56. K. Hadjiivanov, P. Concepción and H. Knözinger, *Top Catal*, 2000, **11**, 123-130.
57. L. Chen, J. Li and M. Ge, *The Journal of Physical Chemistry C*, 2009, **113**, 21177-21184.
58. K. Hadjiivanov and H. Knözinger, *Phys Chem Chem Phys*, 2000, **2**, 2803-2806.
59. R. F. Ilmasani, J. Woo, D. Creaser and L. Olsson, *Industrial & Engineering Chemistry Research*, 2020, **59**, 9830-9840.
60. M. A. Centeno, I. Carrizosa and J. A. Odriozola, *Applied Catalysis B: Environmental*, 2001, **29**, 307-314.
61. Y. Zhang, S. Xu, J. Li, E. He and Z. Liu, *The Journal of Physical Chemistry C*, 2023, **127**, 7248-7256.
62. M. A. Matsko, I. P. Prosvirin, T. B. Mikenas, V. A. Zakharov, E. A. Paukshits, V. I. Bukhtiyarov and I. G. Danilova, *Journal of Molecular Catalysis A: Chemical*, 2000, **158**, 443-446.
63. I. Song, K. Khivantsev, Y. Wang and J. Szanyi, *The Journal of Physical Chemistry C*, 2022, **126**, 1439-1449.
64. H. D. Schmick and H. W. Wassmuth, *Surf Sci*, 1982, **123**, 471-490.
65. K. Hadjiivanov, V. Bushev, M. Kantcheva and D. Klissurski, *Langmuir*, 1994, **10**, 464-471.
66. N. Macleod, R. Cropley and R. M. Lambert, *Catal Lett*, 2003, **86**, 69-75.
67. C.-H. Lin and H. Bai, *Applied Catalysis B: Environmental*, 2003, **42**, 279-287.
68. J. Luo, Y. Tang, S. Joshi, K. Kamasamudram, N. Currier and A. Yezerets, *SAE International Journal of Engines*, 2017, **10**, 1691-1696.

